Mechanistic Investigations on the Heterogeneous Solid-State Reaction of Magnesium Amides and Lithium Hydrides

Ping Chen,*,† Zhitao Xiong,† Lefu Yang,† Guotao Wu,† and Weifang Luo‡

Department of Physics, Faculty of Science, National University of Singapore, 10 Kent Ridge Crescent, Singapore 117542, and Sandia National Laboratories, MS 9403, Livermore, California 94550

Received: March 10, 2006; In Final Form: May 14, 2006

Isothermal and non-isothermal kinetic measurements on the chemical reaction between $Mg(NH_2)_2$ and LiH, as well as the thermal decomposition of $Mg(NH_2)_2$, give apparent activation energies of 88.1 and 130 kJ/mol, respectively, which reveal that the thermal decomposition of $Mg(NH_2)_2$ is unlikely to be an elementary step in the chemical reaction of $Mg(NH_2)_2$ and 2LiH. The H−D exchange between $H^{\delta+}$ in $Mg(NH_2)_2$ and $D^{\delta-}$ in LiD gives evidence for the coordinated interaction between amide and hydride. The observed linear and nonlinear kinetic growth in the reaction of $Mg(NH_2)_2$−2LiH indicates that the reaction rate is controlled by the interface reaction in the early stage of the reaction and by mass transport through the imide layer in the later stage. Both particle size and degree of mixing of the reacting species affect the overall kinetics of the reactions.

1. Introduction

Among all variables that affect the kinetics of a heterogeneous solid-state reaction, mass transport and reaction at the surface or interface(s) are the two common rate-determining processes.[1−3] In a metal hydride system, hydrogen absorption first encounters a surface reaction—chemisorption and dissociation of H_2— and, second, H diffusion from the surface to the bulk. H desorption is the reverse process of absorption.[4]

With ever increasing demand for efficient hydrogen storage materials, more and more research activities have been directed to complex chemical hydrides,[5] metal−N−H,[6−10] and other multicomponent systems.[11] Multistep chemical processes are involved in these systems. $NaAlH_4$, as an example, decomposes to NaH and Al through a two-step process accompanied by sequential phase changes.[5] Similarly, $LiNH_2$−2LiH converts to lithium nitride through stepwise reactions.[6] The rates of mass transport and the reaction at the interface will, inevitably, change with the variation of phases and boundaries.

Reversible hydrogen storage was observed in a Li−Mg−N−H ternary system at a temperature around 180 °C.[7−9] The overall process can be described as:

$$\underset{5.5\ \text{wt}\ \%\ H_2}{Mg(NH_2)_2 + 2LiH \leftrightarrow Li_2MgN_2H_2 + 2H_2} \qquad \Delta H = 44.3\ \text{kJ/mol}\ H_2\ ^{10} \qquad (1)$$

There are two interpretations proposed in the literature for the reaction mechanism.[7,9,10] One is the ammonia-mediated mechanism, in which $Mg(NH_2)_2$ decomposes to ammonia and imide/nitride, depending on temperature (reaction 2), and then the ammonia formed reacts with hydride to produce hydrogen (reaction 3).[9]

$$3Mg(NH_2)_2 \rightarrow 3MgNH + 3NH_3 \rightarrow Mg_3N_2 + 4NH_3 \qquad (2)$$

$$LiH + NH_3 \rightarrow LiNH_2 + H_2 \qquad (3)$$

The observed thermal decomposition of $Mg(NH_2)_2$ at elevated temperatures and the fast reaction between NH_3 and LiH were used as supporting evidence for this interpretation. The other proposed mechanism is the coordinated two-molecule or multimolecular reaction mechanism.[7,10] It is known that the H atoms in $Mg(NH_2)_2$ ($H^{\delta+}$) and LiH ($H^{\delta-}$) possess opposite charges;[12,13] a kind of dihydrogen bonding[14] (or proton−hydride bonding) is likely to occur. There are considerable investigations on the dihydrogen bonding previously.[14−16] In the ammonia−borane (BH_3NH_3) system the intermolecular distance of NH···H−B is ∼1.82 Å, substantially shorter than twice the van der Waals radius of a hydrogen atom, evidencing the establishment of dihydrogen bonds.[17] Simulation shows that the dihydrogen bonds formed in the dimer of AlH_3NH_3 lead to a C_2 symmetrical structure.[18] It is reasonable to deduce that in the hydride−amide system, similar dihydrogen bonding may form during the reaction, which benefits the formation of H_2. Moreover, $N^{\delta-}$ in the amide may interact with the $Li^{\delta+}$ in the hydride, which benefits the setting up of a Li−N bond and the dissociation of a Li−H bond. The overall interactions would favor the formation of $Li_2MgN_2H_2$ and H_2.[7,10] Because Li−Mg−N−H has relatively high hydrogen content and attractive thermodynamics for hydrogen storage,[7,8,10] it has been regarded as one of the promising solid-state materials for on-board hydrogen storage. It is of both practical importance and scientific interest to elucidate the details of the reaction kinetics and mechanism. In the present paper both isothermal and non-isothermal kinetic measurements have been carried out to determine the rate constants of reactions 1 and 2. Designed experiments including isotopic exchange and particle-size effects were carried out to obtain information about mass transport and interface reactions. On the basis of the information obtained in this study, a mechanistic interpretation is proposed for hydrogen desorption from $Mg(NH_2)_2$−2LiH system.

* Corresponding author. Telephone: 65-65162982. Fax: 65-67776126, E-mail: phychenp@nus.edu.sg.
† National University of Singapore.
‡ Sandia National Laboratories.

10.1021/jp061496v CCC: $33.50
Published on Web 07/01/2006

2. Experimental Section

2.1. Sample Preparation. LiH was supplied by Aldrich with a purity of 95%. $Mg(NH_2)_2$ was synthesized onsite by reacting premilled Mg powder with NH_3 at a temperature of 310 °C for 2 days. Its purity is estimated to be above 95%.

Four $Mg(NH_2)_2-2LiH$ samples were prepared. Sample I was prepared by thoroughly ball-milling $Mg(NH_2)_2$ and LiH in a planetary ball mill for 20 h followed by dehydrogenation to 250 °C and rehydrogenation at 180 °C and 80 bar of H_2 for 10 h. Sample II was prepared via a two-step process: first, $Mg(NH_2)_2$ and LiH powder were ball-milled separately for 20 h under the conditions described above; then, the premilled $Mg(NH_2)_2$ and LiH powders were mixed in the same ball mill for 2 h. Sample III underwent the same treatment as sample II except that the mixing of the premilled amide−hydride was carried out by a mortar−pestle for 10 min. Sample IV was made by directly mixing as-received $Mg(NH_2)_2$ and LiH in a mortar−pestle for 10 min. Sample I was used for isothermal and non-isothermal kinetic tests.

Isotopic exchange testing was performed over two samples. One was a $Mg(NH_2)_2-2LiD$ ($Mg(NH_2)_2/LiD = 1/2$) sample, ball-milled for 10 h; the other one was a $Li_2MgN_2H_2-LiD$ ($Li_2MgN_2H_2/LiD = 1/1$) sample, milled for 10 h too. $Li_2MgN_2H_2$ powder was synthesized by dehydrogenation of $Mg(NH_2)_2-2LiH$ (sample I) to 250 °C.

All the sample loading and mixing were conducted in an Ar-filled glovebox (M BRAUN).

2.2. Kinetic Measurements. An intelligent gravimetric analyzer (IGA, Hiden) was employed to monitor the sample weight changes with time and temperature. Both reactions 1 and 2 release gaseous products. The extent of the reaction was calculated from the weight loss of the sample. The testing chamber was kept at a vacuum of at least 10^{-4} mbar to remove the gaseous products effectively. Both isothermal and non-isothermal approaches were adopted. In the isothermal mode, the sample was quickly heated to and kept at a given temperature. The sample weight was monitored as a function of time by a microbalance. In the non-isothermal testing, the sample was gradually heated to a given temperature at a linear ramping rate of 0.5 °C/min. Approximately 150 mg of $Mg(NH_2)_2-2LiH$ (sample I) and $Mg(NH_2)_2$ samples were tested. The sample temperature was measured by a thermocouple placed ~0.2 cm above the sample. The temperature resolution is within ±0.1 °C.

2.3. FTIR Measurement. The N−H and N−D vibrations of the samples were determined by a Perkin-Elmer system 2000 FTIR, where 32 scans were accumulated. The scan resolution was 4 cm^{-1}. The sample was loaded to an in situ DRIFT cell in a glovebox.

2.4. TPD Measurement. A homemade temperature-programmed-desorption (TPD) system was employed to detect the size effect and degree of mixing of the reactant on the reaction kinetics.[6] The TPD system is composed of a microreactor, a mass spectrometer and a gas chromatograph. A sample of 100 mg was employed for each measurement. Purified Ar was used as carrier gas, and the temperature ramping rate was 2 °C/min.

3. Results and Discussions

3.1. Kinetic Investigations.

3.1.1. Isothermal Testing. Kinetic expressions for solid-state reactions can be generally described by

$$r = d\alpha/dt = k(T)f(\alpha) \quad (4)$$

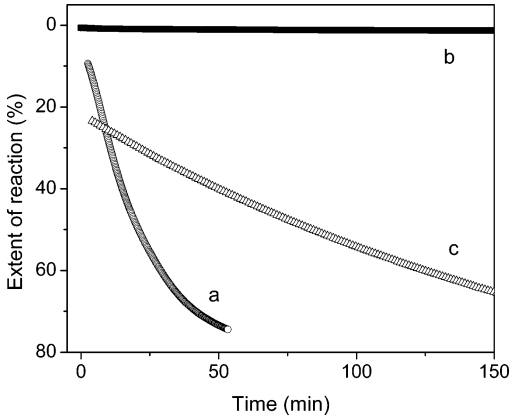

Figure 1. Time dependences of the extent of the reaction of $Mg(NH_2)_2-2LiH$ at 163 °C (a); thermal decomposition of $Mg(NH_2)_2$ at 167 (b) and 275 °C (c), respectively.

where r is the reaction rate, α is the extent of reaction, t represents time, T is temperature, $k(T)$ is a temperature-dependent rate constant, and $f(\alpha)$ is the function that relates to a reaction model. $k(T)$ can be determined by knowing the relationship between r and $f(\alpha)$.

Figure 1 shows the time dependences of the extents of reaction 1 at 163 °C and reaction 2 at 167 and 275 °C, respectively. It can be seen that the $Mg(NH_2)_2-2LiH$ sample quickly releases hydrogen at 163 °C. The extent of reaction reaches 76% within the first 60 min. However, $Mg(NH_2)_2$ hardly decomposes to NH_3 at 167 °C. After 150 min heating, the $Mg(NH_2)_2$ decomposition is still below 1.4%. Increasing the temperature to 275 °C, the decomposition reaches 65% after 150 min. It should be noted that high vacuum has been applied to all tests; therefore, the reversed reactions of 1 and 2 can be excluded.

It can be seen in Figure 1 that the evolutions of curves display both linear and nonlinear relationships between α and time. The linear relationship is followed until α reaches ~25% for reaction 1 and ~40% for reaction 2. The nonlinear part somehow exhibits an exponential decay behavior. The physical meanings of the linear and nonlinear growth will be discussed in the later part of this paper. On the basis of the linear relationship between time and the extent of the reaction, we can assume that reactions 1 and 2 maintain relatively constant rates during the initial part of these reactions and, therefore, zero-order rate law can be applied. This can further be used to determine the rate constant at given temperatures according to

$$r = d\alpha/dt = k(T) \quad (5)$$

A $k(T)$ can be determined by one isothermal test run. To calculate the Arrhenius constants a number of isothermal runs are needed. There is a major experimental problem associated with the isothermal method; i.e., a sample has to pass a non-isothermal process, i.e., the ramping period, before reaching the preset temperature. During this period the sample may undergo unwanted transformation, which is likely to affect the result of analysis. Non-isothermal analysis can resolve this problem. On the other hand, sufficient data can be obtained to determine the kinetic parameters by non-isothermal test.[19]

3.1.2. Non-isothermal Kinetic Measurements. To derive kinetic parameters of reactions 1 and 2 from the non-isothermal kinetic investigations, the extent of the reaction was kept below 25%, where the linear relationship between time and the extent of the reaction exists (see Figure 1). Furthermore, a constant heating rate was set to be as slow as 0.5 °C/min. Figure 2 shows

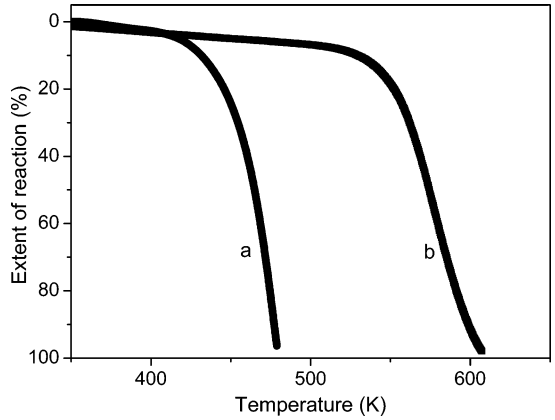

Figure 2. Temperature dependence of the extent of the reaction of $Mg(NH_2)_2-2LiH$ (a) and the thermal decomposition of $Mg(NH_2)_2$ (b).

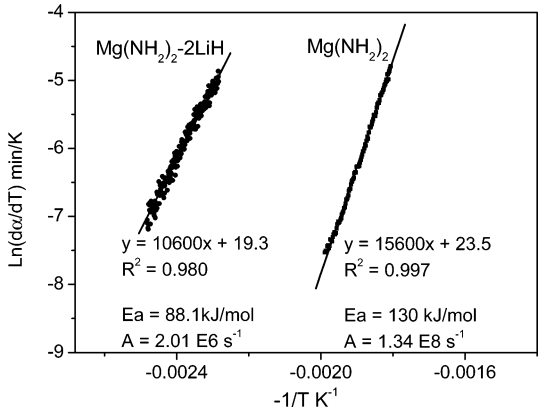

Figure 3. Arrhenius plot of rate constants derived from Figure 2. The linear fits yield activation energies and preexponential factors.

the temperature dependence on the extent of reactions 1 and 2. It can be seen that detectable reaction rate was observed at temperatures above 120 °C for reaction 1 and 230 °C for reaction 2. Since the temperature was increased at a constant rate, eq 5 can be transformed into

$$r = \mathrm{d}\alpha/\mathrm{d}t = \beta\, \mathrm{d}\alpha/\mathrm{d}T = k(T) \tag{6}$$

where β is the heating rate, $\beta = \mathrm{d}T/\mathrm{d}t$. Further transforming eq 6 into Arrhenius form, we have

$$\mathrm{d}\alpha/\mathrm{d}T = k(T)/\beta = (A/\beta)\mathrm{e}^{-E_a/RT} = A'\mathrm{e}^{-E_a/RT} \tag{7}$$

$$A' = A/\beta$$

Figure 3 is the plot of $\ln(\mathrm{d}\alpha/\mathrm{d}T)$ vs $-1/T$ for the temperature ranges of 130−165 and 230−280 °C for reactions 1 and 2, respectively, where the extents of reactions 1 and 2 are all below 25%; in other words, the linear growth is followed. A high degree of linearity of $\ln(\mathrm{d}\alpha/\mathrm{d}T)$ and $-1/T$ (with $R^2 = 0.980$ for $Mg(NH_2)_2-2LiH$ and 0.997 for $Mg(NH_2)_2$) were observed, which further validates the assumption of zero-order rate law. From the slopes and intercepts of the two fitted lines, the activation energies and preexponential factors of the two reactions were determined. As shown in Figure 3, the apparent activation energies for reactions 1 and 2 are 88.1 and 130 kJ/mol and the corresponding preexponential factors (A) are 2.01×10^6 and 1.34×10^8 s^{-1}, respectively (±5% of measurement error is estimated). The reaction rates of reactions 1 and 2 are given below:

$$r_1 = 2.01 \times 10^6 \mathrm{e}^{-88100/RT} \tag{8}$$

$$r_2 = 1.34 \times 10^8 \mathrm{e}^{-130000/RT} \tag{9}$$

It should be noted that the equations above are only applicable to the part of the reaction wherein the linear relationship between α and time exists.

The rather large activation energy measured for the thermal decomposition of $Mg(NH_2)_2$ reveals that $Mg(NH_2)_2$ has to pass through a higher energy barrier to liberate NH_3. On the other hand, hydrogen desorption from the mixture of $Mg(NH_2)_2$ and 2LiH encounters lower energetic resistance. Clearly, a more energy-favorable pathway is adopted by reaction 1. It is calculated from eqs 8 and 9 that reaction 1 occurs at a much faster rate than reaction 2 at temperatures below 700 °C. For a chemical process, the apparent reaction rate normally should equal that of the rate-determining elementary step,[20] therefore, thermal decomposition of $Mg(NH_2)_2$ is unlikely to be an elementary step in reaction 1, especially at lower temperatures. If reaction 1 is, however, operated at higher temperatures, where reaction 2 can proceed with an appropriate rate, the NH_3-mediated pathway may somehow contribute to the overall reaction rate.

There was an argument on the catalytic effect of hydride on the thermal decomposition of amide; i.e., the decomposition of amide can be catalyzed by the other reactant−hydride.[9] If LiH does work as catalyst, the immediate implication is the formation of a transition state with lower kinetic barrier between amide and the catalyst−hydride molecules−which weakens the existing chemical bonds, such as Mg−N, and/or promotes the formation of new bonds. All these changes should come from a kind of chemical interaction between amide and the catalyst (hydride) molecules. The questions here are what the nature of this interaction should be and why such interaction does not lead to the more thermodynamically favored products (imide and hydrogen), but rather to ammonia, magnesium imide, and unreacted hydride molecule.

It should be noted that the activation energy of reaction 1 determined by Kissingner's method ($E_a = 102$ kJ/mol) previously[10] is ∼15% higher than that of the present investigation, which is understandable, since in Kissinger's method the reaction rates adopted are those in or near the middle of the reaction, wherein the linear relationship between α and time does not exists. As for reaction 2, the data derived by both methods are comparable because the linear relationship between α and time holds within a much larger range of α.

3.2. Origin of Kinetic Barrier. Previous thermodynamic analysis predicts that reaction 1 can take place at temperatures around 90 °C at 1.0 bar hydrogen pressure,[10] indicating that it should proceed at even lower temperatures when high vacuum is applied. The experimental results revealed, however, that a measurable reaction rate was observed only at temperatures greater than 120 °C (see Figure 2) due to the relatively higher kinetic barrier demonstrated above. It is important to investigate the origin of the barrier in order to provide information for the material engineering.

As mentioned above, a heterogeneous solid-state reaction normally consists of, at least, two components, i.e., interface reaction and mass transport.[1] Regardless of the morphologies of the grains and interfaces, Scheme 1 generally applied in a heterogeneous solid-state reaction can be used to qualitatively describe the process of the amide−hydride interaction.

Initially the reaction occurs at the interface of the amide and hydride. When the reaction proceeds, the product layer formed

SCHEME 1: Chemical Reactions at the Interfaces of Amide/Hydride, Amide/Imide, and Imide/Hydride and Mass Transport through the Imide Layer

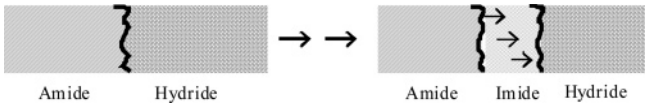

thickens gradually, and therefore, the interface reactions actually take place at the phase boundaries of hydride/imide and imide/amide. Mass transport of the reacting ions carries on through the product layer.

To identify the origin of the kinetic barrier, three experiments were designed and the results are shown below.

3.2.1. Imide Formation and H−D Isotopic Exchange at the Interface of Magnesium Amide and Lithium Deuteride. $Mg(NH_2)_2$ and LiD were ball-milled in a molar ratio of 1/2 at ambient temperature and in an Ar atmosphere. The estimated local temperature during ball-milling is ~50 °C. The pressure within the ball-mill vessel increased from 14 to 17 psi after 10 h of ball-milling. The gaseous content in the vessel includes Ar, H_2, HD, and D_2, which was identified by a mass spectrometer (see Figure 4). Our previous investigations demonstrated that when pure LiD or $Mg(NH_2)_2$ was ball-milled alone, no gaseous product can be detected. The chemical composition of the solid residue remains unchanged. Therefore, the appearance of H_2, HD, and D_2 reveals the occurrence of reaction 1. By calculation, 3 psi of hydrogen gas is equivalent to ~2% of conversion of reactants. The postmilled sample was collected and measured by IR in diffuse reflectance infrared Fourier transform (DRIFT) mode. N−H and N−D stretches were observed. As shown in Figure 5, symmetric and asymmetric N−H stretches of the $Mg(NH_2)_2$ molecule give two strong absorbances at 3271 and 3324 cm^{-1}, respectively. Imide is clearly detected with a corresponding N−H stretch at 3187 cm^{-1}, further evidencing the occurrence of reaction 1. Another interesting feature observed in the IR spectrum is the development of a new absorbance at 2433 cm^{-1} assignable to the N−D stretch in deuterium-substituted magnesium amide, which is evidence for the occurrence of H−D exchange between the $Mg(NH_2)_2$ and LiD. This is a strong support for the coordinated mechanism of reaction 1;[7,10] i.e., only when amide and hydride form a bimolecular or trimolecular transition state through a dihydrogen bonding, can H and D be close enough for H−D exchange. The Coulombic attraction between H and D with opposite charges would help the establishment of the transition state as mentioned above.

It is worth mentioning that the H−D exchange during reaction 1 will bring complications (i.e., isotopic effect) to the attempts in identifying the reaction mechanism by quantitatively measuring the gaseous products, i.e., the relative amount of H_2, HD, and D_2.[21,22] The observed distribution of the desorbed gases is actually the results of multiple H−D exchanges among solid reactants, products and gaseous products, which is strongly influenced by the reaction conditions, such as temperature, gas flow rate, and thickness of reacting layer, etc. Unless equilibrium is achieved, the composition of the gaseous products may mainly reflect the dynamic results of the H−D exchange.

3.2.2. Reactions at the Interfaces of Imide/Hydride and Imide/Amide. As reaction 1 proceeds, the product, imide, layer is gradually developed between amide and hydride phases. The interface reaction, therefore, consists of both reactions at the amide/imide and imide/hydride phase boundaries. Basically, the reaction at the interface of imide/hydride or imide/amide may consist of the following steps: (I) transport of reacting species, i.e., Li, Mg, N, and H, across the interface; (II) ordering of chemical species across the interface; (III) structural transformation and other associated phenomena.[2] In general, at the initial stage of a multiphase solid-state reaction, the reaction rate is determined by the interface reaction wherein the kinetic barrier of mass transport through a very thin product layer can be negligible.[1,23−25] If the properties of the interface remain essentially unchanged, a linear growth law will be obeyed.[1,23−25] Such a linear growth was indeed observed in reaction 1 (see Figures 1 and 3), revealing that the interface reaction is the rate-limiting step during the initial part of desorption. As there are two interfaces in the reacting system with different compositions and structures, the reaction kinetics may not be identical to each other. We investigated the interface reaction between imide and hydride by looking at the H−D isotopic exchange between $Li_2MgN_2H_2$ and LiD. Results show that considerable H−D exchange occurs during ball-milling (see Figure 5). The intensity of the N−D stretch is ~40% of that of the N−H stretch, indicating the fairly easy occurrence of H−D exchange, which further indicates the relatively lower kinetic barrier for imide and hydride to establish a reacting transition state. Although more quantitative measurements are needed, the reaction at the imide/hydride interface is probably not the rate-determining step. On the other hand, the complex mass transport across the phase boundary may cause the reaction at the imide/amide interface to be the rate-determining step.[26] Detailed investigations are being conducted.

It should be mentioned that the pattern of a desorption curve depends on the particle size, as well as the degree of mixing of

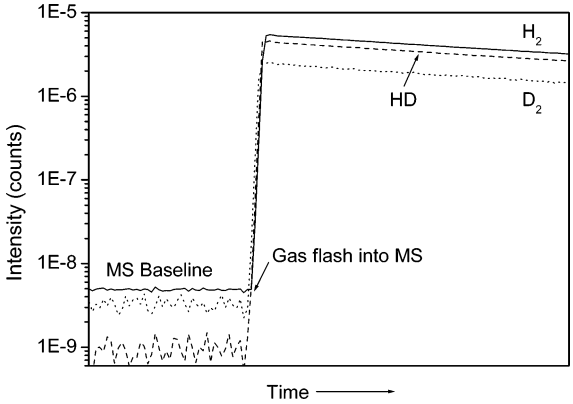

Figure 4. Gaseous composition within the ball-mill vessel, which was detected by a mass spectrometer. A baseline was run prior to the introduction of gases from the ball-mill vessel. Signals of H_2, HD, and D_2 have been modified by the relative sensitive factors.

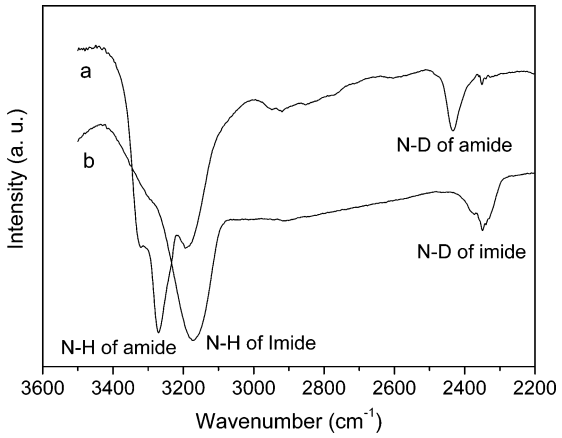

Figure 5. DRIFT spectra of the ball-milled $Mg(NH_2)_2$−2LiD sample (a) and the $Li_2MgN_2H_2$−LiD sample (b).

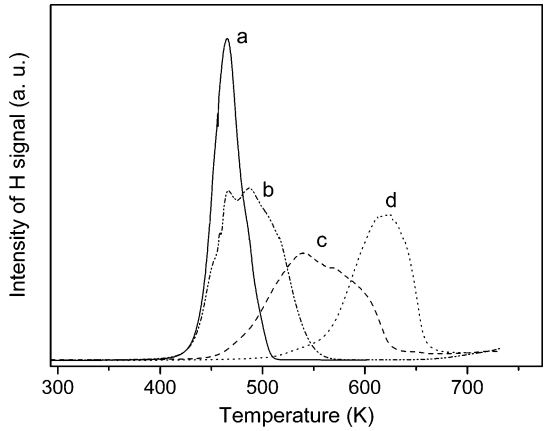

Figure 6. Temperature-programmed desorption of $Mg(NH_2)_2-2LiH$ sample I (a), sample II (b), sample III (c), and sample IV (d).

the two reacting species in a sample. The relatively longer linear part of the disorption profile, (shown in Figure 1a, up to 25% of a full desorption, for reaction 1) can be attributed to the thorough pre-ball-milling treatment, resulting in sub-micrometer-sized (<500 nm) particles and sufficient contact of reactants.

3.2.3. Mass Transport through Product Layer. The product, imide, layer grows with desorption advancing. The resistance of mass transport through this thickening imide layer could finally surpass the barrier of the interface reaction, upon which mass transport through the imide layer becomes the rate-determining process. A parabolic growth was observed in the isothermal investigation of reaction 1, as shown in the nonlinear part of Figure 1a.

It should be noted that the physical state of reactants, such as particle size and degree of mixing, etc., greatly affect the overall kinetics of reaction 1. To investigate the effect of particle size and degree of mixing, four samples were prepared for TPD testing (see section 2.1). Particle sizes are comparable (<500 nm) for samples I−III since they were prepared under similar milling conditions; sample IV has a relatively large particle size (>100 μm). The differences among samples I−III lie in the degree of mixing between two reacting species. As can be interpreted from the preparation process, the degree of mixing is in the sequence of sample I > sample II > sample III. It can be seen from the TPD results in Figure 6 that sample I shows the fastest kinetics, i.e., the lowest peak temperature and the shortest time to complete a full desorption. Sample II is next, and sample III is even worse. For sample IV, hydrogen desorption can be observed only at a temperature > 230 °C. Clearly, poor mixing between two reacting species will result in less chance of direct interaction between amide and hydride and a longer mass transport distance and, consequently, the reaction rate becomes slower. Under the extreme condition where the contact between two reacting species in the solid is minimized (such as that of sample IV), the ammonia-mediated reaction pathway may play an important role in the hydrogen desorption from $Mg(NH_2)_2-2LiH$.

Conclusions

Isothermal and non-isothermal kinetic measurements on the chemical reaction between $Mg(NH_2)_2$ and LiH, as well as the thermal decomposition of $Mg(NH_2)_2$, give apparent activation energies of 88.1 and 130 kJ/mol, respectively. The considerable differences in the Arrhenius parameters between these two chemical processes reveal that the thermal decomposition of $Mg(NH_2)_2$ is unlikely to be an elementary step in the chemical reaction of $Mg(NH_2)_2-2LiH$. The ammonia-mediated mechanism is, therefore, energetically unfavorable. Isotopic exchange investigations are supportive to the coordinated mechanism.

The observed linear relationship between time and the extent of the reaction of $Mg(NH_2)_2-2LiH$ indicates that the kinetic barrier may come from the interface reaction in the earlier stage of the reaction. As the reaction proceeds, resistance of mass transport through the product layer increases and it becomes the rate-determining step. The particle size and the degree of mixing of reacting species will affect the overall kinetics.

Acknowledgment. The present work is financially supported by Agent for Science, Technology and Research (A*STAR, Singapore). Thanks from W. Luo for the funding provided by the Department of Energy, Office of Energy Efficiency and Renewable Energy, under the Hydrogen Storage Grand Challenge, Center of Excellence within DOE's National Hydrogen Storage Project.

References and Notes

(1) Schmalzried, H. *Solid State Reactions*; Verlag Chemie: Weinheim, Germany, 1981.
(2) Backhaus-Ricoult, M. *Annu. Rev. Mater. Res.* **2003**, *33*, 55.
(3) Borg, R. J.; Dienes, G. J. *The Physical Chemistry of Solid*; Academic Press: San Diego, CA, 1992.
(4) Wang, X. L.; Suda, S. *J. Less-Common Met.* **1990**, *159*, 83.
(5) Bogdanovic, B.; Schwickardi, M. *J. Alloys Compd.* **1997**, *253*, 1.
(6) Chen, P.; Xiong, Z. T.; Luo, J. Z.; Lin, J. Y.; Tan. K. L. *Nature* **2002**, *420*, 302.
(7) Xiong, Z. T.; Wu, G. T.; Hu, J. J.; Chen, P. *Adv. Mater.* **2004**, *16*, 1522.
(8) Luo, W. F. *J. Alloys Compd.* **2004**, *381*, 284.
(9) Leng, H. Y.; Ichikawa, T.; Hino, S.; Hanada, N.; Isobe, S.; Fujii, H. *J. Phys. Chem. B* **2004**, *108*, 8763.
(10) Xiong, Z. T.; Hu, J. J.; Wu, G. T.; Chen, P.; Luo, W. F.; Gross, K. *J. Alloys Compd.* **2005**, *398*, 235.
(11) Gutowska, A.; Li, L. Y.; Shin, Y. S.; Wang, C. M. M.; Li, X. H. S.; Linehan, J. C.; Smith, R. S.; Kay, B. D.; Schmid, B.; Shaw, W.; Gutowski, M.; Autrey, T. *Angew. Chem., Int. Ed.* **2005**, *44*, 3578.
(12) Sapse, A. M.; Jain, D. C.; Raghavachari, K. R. *Lithium Chemistry*; Wiley: New York, 1995.
(13) Yamamura, S.; Kasahara, S.; Takata, M.; Sugawara, Y.; Sakata, M. *J. Phys. Chem. Solids* **1999**, *60*, 1721.
(14) Custelcean, R.; Jackson, J. *Chem. Rev.* **2001**, *101*, 1963.
(15) Crabtree, R. H. *Science* **1998**, *282*, 2000.
(16) Calhorda, M. J. *Chem Commun. (Cambridge)* **2000**, 801
(17) Richardson, T. B.; de Gala, S.; Crabtree, R. H.; Siegbhan, P. E. M. *J. Am. Chem. Soc.* **1995**, *117*, 12875.
(18) Cramer, C. J.; Gladfelter, W. L. *Inorg. Chem.* **1997**, *36*, 5358.
(19) Vyazovkin, S.; Weight, C. A. *Int. Rev. Phys. Chem.* **1998**, *17*, 403.
(20) Benson, S. W. *The Foundations of Chemical Kinetics*; McGraw-Hill: New York, 1962.
(21) Chen, P.; Luo, J. Z.; Xiong, Z. T.; Lin, J. Y.; Tan, K. L. *J. Phys. Chem. B* **2003**, *107*, 10967.
(22) Isobe, S.; Ichikawa, T.; Hino, S.; Fujii, H. *J. Phys. Chem. B* **2005**, *109*, 14855.
(23) Erukhimovitch, V.; Baram, J. *Phys. Rev. B* **1995**, *51*, 6221.
(24) Chen, J. C.; Shen, G. H.; Chen, L. J. *J. Appl. Phys.* **1998**, *84*, 6083.
(25) Ressler, T.; Wienold, J.; Jentoft, R. E.; Neisius, T.; Gunter, M. M. *Top. Catal.* **2002**, *18*, 45.
(26) Luo, W. F.; Sickafoose, S. *J. Alloys Compd.* **2006**, *407*, 274.